JACS Au
AN OPEN ACCESS JOURNAL OF THE AMERICAN CHEMICAL SOCIETY

pubs.acs.org/jacsau
Article

Split Syntheses: Introducing Bottom-Up Control over Aluminum in SSZ-13 and ZSM-5 Zeolites

Sven Robijns, Julien Devos, Beatrice Baeckelmans, Tom De Frene, Mostafa Torka Beydokhti, Rodrigo de Oliveira-Silva, Niels De Witte, Dimitrios Sakellariou, Tom R. C. Van Assche, and Michiel Dusselier*

Cite This: JACS Au 2025, 5, 593−605

ABSTRACT: Zeolite synthesis is known as a difficult-to-control process, with many degrees of freedom that have a partially uncharted impact on the final product. Due to this, many zeolite scientists have regarded the initial mixing (aging) stage as the only time at which the chemical composition of a zeolite synthesis mixture can be impacted without heavily disrupting the delicate equilibria that are at play during crystallization. Recently, however, this view has started to change, with innovative techniques such as charge density mismatch or electro-assisted synthesis showing that the addition of new elements to the reactor midsynthesis might lead to new and surprising outcomes. In this manuscript, we show that by intermittent removal of certain fractions, notably Al-rich solids or Si-rich liquids, from the reaction medium during an interzeolite conversion from FAU-to-CHA (and FAU-to-MFI), one can control the Si/Al ratio of the final product, without heavily impacting the reaction time, particle size, or divalent cation capacity of the final product. This approach was named "split synthesis" and has led to several insights. By removing some Si-rich liquid phase after 40 min of synthesis, the Si/Al ratio of the daughter zeolite was lowered to a value of 20 (starting from 40), while the divalent cation capacity, a performance indicator for several acid and metal-catalyzed reactions, was kept maximized. On the other hand, when Al-rich solids were removed after 40 min (and in some cases colloidal silica was supplemented), we were able to rapidly synthesize small SSZ-13 zeolites with Si/Al ratios up to 180. These high-Si SSZ-13 zeolites had particle sizes in the range 100−150 nm and are traditionally difficult to crystallize in hydroxide medium. They showed a great olefin yield (6%) in the conversion of CO_2 and H_2 with ZnZrOx as cocatalyst.

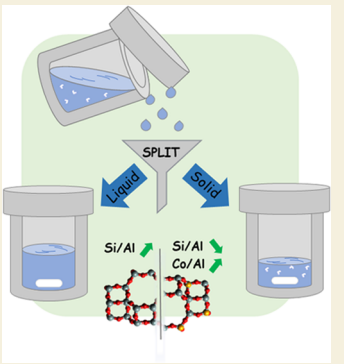

KEYWORDS: *zeolite synthesis, CO_2 conversion, high-silica zeolites, nanosized zeolites, hydrothermal synthesis, CO_2-to-olefins*

1. INTRODUCTION

Zeolites are a class of microporous aluminosilicates which can form naturally in the presence of alkaline (earth) cations at elevated temperatures and pressures.[1,2] Richard Barrer was the first one to mimic this natural process in the lab by synthesizing a synthetic zeolite with no natural counterpart using a batch reactor.[3] Since then, the concept of autoclave-based synthesis of zeolites was born and most variations in the synthesis of these materials were performed through ab initio variations in the batch compositions, i.e., by mixing the components inside of an autoclave and letting them react until the desired product had been formed.[4] Recently, however, a drive toward the synthesis of catalysts with more tuned properties has led researchers to drop the notion that synthesis parameters cannot be changed once the reaction has started and opened up the possibility to make changes in batch composition during hydrothermal synthesis at elevated temperatures.

Some reports showed the viability of changing the batch composition during synthesis, either by reactor-based solutions (e.g., electro-assisted synthesis (EAS) by our lab)[5] or by simply stopping the reaction after a partially completed synthesis, such as is the case with charge density mismatch (CDM) methods.[6] In CDM, an initial mixture of (positively charged) cations and (negatively charged) aluminate species is mixed in such a way that there is an insufficient amount of structure-directing cations to compensate for the charge of negatively charged AlO_2^-. Then, after some synthesis time (or in practice: aging), the charge density barrier is broken by the addition of a second template with higher charge density, sparking rapid nucleation and further crystal growth. However useful this technique has been (e.g., leading to the discovery of UFI),[7] CDM has only been applicable to the synthesis of relatively aluminous zeolites, with Si/Al spanning from 1 up to 10.[1]

Interzeolite conversion (IZC), a synthetic variation of conventional batch synthesis in which an already crystalline mother zeolite is used as a source of T-atoms, has gained traction

Received: June 26, 2024
Revised: October 23, 2024
Accepted: October 24, 2024
Published: January 28, 2025

https://doi.org/10.1021/jacsau.4c00551
JACS Au 2025, 5, 593−605

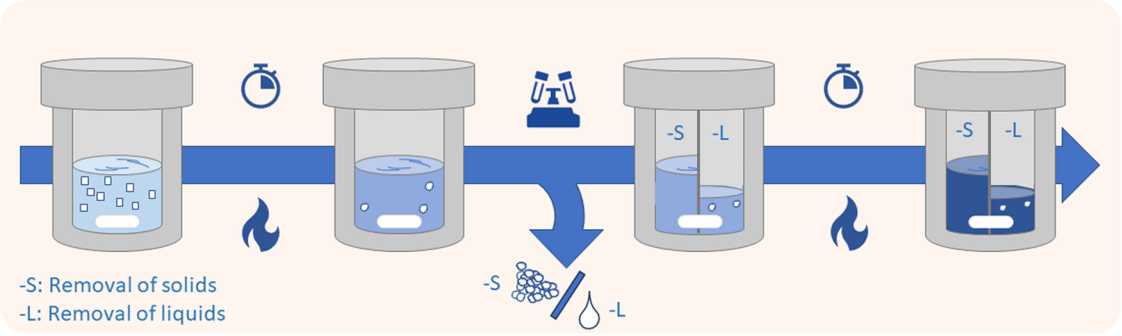

Figure 1. Schematic picture of SPLIT-S (removal of solids) and SPLIT-L (removal of liquids) syntheses.

in the past decade as a promising synthesis technique.[8] It is industrially relevant as it is often capable of rapidly synthesizing small crystals with high yield.[9] Another benefit of IZC compared to the use of conventional (often amorphous) starting materials is the ability to obtain high divalent cation capacity (DCC, often expressed as a molar Co/Al ratio after a relatively mild aqueous Co exchange).[8,10,11] According to Devos et al., this is a direct result of the kinetic nature of IZC, as during the synthesis, a relatively high supersaturation is reached due to the reactive nature of the dealuminated FAU used as a starting source. It thus comes as no surprise that when IZC is employed in combination with more standard techniques for increasing the DCC in SSZ-13, such as the use of charge dense alkali cations,[12−14] the theoretical maximum Co/Al of 0.5 was reached.[15]

Siliceous (Si/Al > 35) IZC is generally observed to pass through 4 stages, which are often not clearly delineated as they overlap.[16] First there is incongruent dissolution of the starting source as silica will dissolve more easily than Al. In the second induction phase, this will lead to the presence of an Al-rich solid, residing inside of a silica-rich liquid in a dynamic equilibrium. Finally, the third phase, crystallization, will rapidly take place once nucleation has occurred (terminating the induction phase), followed by a maturation stage, in which a dynamic equilibrium between solid and liquid is reached again.[17] The concentration of aluminum in an easily separable solid phase during the induction phase begs the question of whether physical manipulations at this point might have some influence on the composition of the final product.

Recently, the synthesis of high-silica SSZ-13 (with Si/Al > 50) in hydroxide medium has been widely sought after as, in general, hydroxide-based synthesis routes are faster and produce smaller crystals than the F^--mediated route. The difficulty-to-synthesize high-silica SSZ-13 can be explained by the observation that CHA is more stable when crystallizing in an aluminous environment compared to more siliceous CHA.[8,18] It is thus surprising that high-silica SSZ-13 zeolites have been synthesized using a plethora of methods including seeding,[19] dry gel conversion,[20] and HF.[21] Especially noteworthy are the efforts of the Cao group, who succeeded in synthesizing a pure silica SSZ-13 zeolite (Si-CHA) in hydroxide media by using both seeds and 4 h of aging.[22] Also the efforts of Liu et al. can be noted, obtaining pure silica CHA through an IZC starting from pure silica SOD in hydroxide medium, through a mechanism involving hetero-epitaxial growth.[23] These reports showcased the possibility of synthesizing pure silica CHA in hydroxide medium and thus motivate high-silica SSZ-13 as an initial target for investigating a diverse range of FAU-to-SSZ-13 interconversions by a novel synthetic method, named hereafter, the "split synthesis".

In this technique, an FAU-to-CHA IZC recipe as described by Robijns et al.[15] is employed; however, the synthesis itself is interrupted after ∼40 min of thermal activation (or high temperature aging for the critics). After this, the alumina-rich solid phase and the silica-rich liquid phase are separated (split), and fractions of each are recombined and allowed to react further by inserting them in an oven at 160 °C (Figure 1). This seemingly simple concept is shown here to be an excellent tool to control the Si/Al without significantly altering other properties of the resulting zeolites, such as DCC or particle size.

2. MATERIALS AND METHODS

2.1. Zeolite Synthesis

The synthesis of zeolites was based on an earlier report by Robijns et al.[15] However, in this work, zeolites were synthesized through the so-called split synthesis. In this procedure, 12.55 g of a 20 wt % N,N,N-trimethyladamatylammonium hydroxide (TMAdamOH, Sachem) was mixed with 0.57 g of an aqueous 10 wt % LiOH (98% Anhydrous, Acros Organic) solution and 1.55 g of MQ water (18.2 mΩ). Next, under magnetic stirring, 2.5 g of CBV780 (Si/Al = 40, H-form, Zeolyst, used as delivered) is added to the solution. In general, the resulting batch composition is 1 SiO2:0.025 AlO_2^-: (0.35-X) $TMAdam^+$:X Li^+: 0.35 OH^-: 17.5 H_2O, with X = 0−0.06. The solution is mixed for 5 min at 500 rpm (heat-resistant multiposition stirring plate, 2mag) to homogenize and transferred to a PTFE-lined steel autoclave (Parr Instruments, 23 mL acid digestion vessel), after which the autoclave is placed in a forced convection oven (Heratherm, Thermo Scientific) at a temperature of 160 °C under 600 rpm of stirring. When a split synthesis is performed, the autoclave is taken out of the oven after exactly 40 min of synthesis and placed in a cooling bath with fresh (cold) tap water (∼15 °C) for 10 min to rapidly quench the mixture. While the vessel can still feel a bit warm to the touch, it is opened, and the contents are fully transferred to a polypropylene centrifuge tube (50 mL PP tube, Sarsted). The PTFE liner is thoroughly rinsed with MQ water and dried with a paper towel, in order to wash away any remaining residue and avoid the transfer of unwanted liquid or solid fractions. The PP tube is centrifuged for 10 min at 6700 rpm (Thermo Fisher Scientific, SL16) after which the liquids can be decanted and separated from the solids. Next, fractions of the liquid and solid phases (depending on the nature of the synthesis this might be only the liquid phase (SPLIT-S) or a mix of the liquid and solid phase (SPLIT-L)), together with any additional amount of silica added in the form of colloidal silica (SPLIT-S + Col), are placed into the (dry) original PTFE liner, after which the mixture is stirred for 5 min at 600 rpm, capped and placed back into the oven at 160 °C for 20 h. (*Note: To avoid confusion on the exact nature of a sample, the naming (e.g., SPLIT-S + Col) was based on mathemathical operators where − (minus) was used to indicate the removal of a fraction from the batch and + (plus) was used to indicate addition*) After this, the autoclave is once more cooled in a cold-water bath. A schematic representation of this procedure is shown in Figure 1. The content of the autoclave was transferred into a 50 mL PP centrifuge tube and centrifuged for 20 min at 6000 rpm. The liquid was decanted, while the solid was washed. For

https://doi.org/10.1021/jacsau.4c00551
JACS Au 2025, 5, 593−605

the washing of the solid phase, ∼35 mL of deionized water was added to the centrifuge tube, after which it was shaken to bring all solids into suspension. Next, the mixture was centrifuged for 20 min at 6000 rpm, and all liquids were decanted and discarded. This procedure was repeated at least 3 times until the pH of the mixture dropped below 9. Finally, the solids were washed one last time with 20 mL of acetone and kept in an oven at 60 °C overnight for drying.

Reference samples were synthesized through standard IZC (i.e., an IZC without interrupting the synthesis and without performing a split at 40 min) using different starting sources (CBV720 (Si/Al = 15), CBV760 (Zeolyst, Si/Al = 30) or HSZ-390HUA (TOSOH, Si/Al > 300)) depending on the required batch composition. Aside from small changes resulting from the presence of water in the used zeolites, used weights of reagents were similar to the ones used in the split procedure. The resulting batch compositions were 1 SiO_2: X AlO_2^-: 0.35 $TMAdam^+$: 0.35 OH^-: 17.5 H_2O, with X = 0.067, 0.033, or 0.003 depending on the Si/Al of the mother FAU. After mixing the FAU with 20 wt % *N,N,N*-trimethyladamatylammonium hydroxide and water, the autoclave was sealed, and the reaction was left to proceed at 160 °C for up to 2 days. Subsequent washing and calcination were similar to those listed for the split procedure above.

2.2. Calcination

The dried solids are calcined to remove the OSDA and free the pores for further analysis. This is achieved by heating the powder in a muffle oven to 580 °C with a ramp of 1 °C/min under air (LV9/11, Nabertherm). After, these zeolites are transferred into a closed container to mitigate the uptake of water from the atmosphere. Weights before and after calcination are noted down.

2.3. Ion Exchange

For the determination of the DCC, an ion exchange was conducted. First, the calcined zeolite is suspended in 150 mL/g of a 0.5 M solution of NaCl (>99%, VWR). The mixture is stirred at 600 rpm for a certain time after which it is centrifuged, and liquids are decanted. This procedure is repeated three times for 16, 8, and 16 h, respectively. Next, the same procedure is repeated further three times, this time using 150 mL/g of a 0.05 M $Co(NO_3)_2$ solution (>99%, Acros Organics). Finally, the sample is washed three more times with MQ water to rinse off the excess cations and is dried at 60 °C overnight.

2.4. X-ray Powder Diffraction

The structure and crystallinity of the noncalcined zeolites were confirmed by X-ray powder diffraction (PXRD) on a high-throughput STOE STADI P Combi diffractometer in transmission mode with focusing Ge(111) monochromatic X-ray inlet beams (λ = 1.5406 Å, Cu Kα source). For each sample, a beam time of 10 min is used. *Note: All samples displayed in this work were fully crystalline unless mentioned otherwise.*

2.5. Nitrogen Physisorption

Porosity is measured by nitrogen physisorption (Tristar II 3020, micromeritics) at −196 °C on calcined and dried samples (≥6 h at 300 °C). The relative nitrogen pressure is varied between 0.01 and 0.99 (p/p_0). The *t*-plot method (Harkins and Jura) on the adsorption branch is used to determine micropore volumes.

2.6. Elemental Analysis

Before inductively coupled plasma atomic emission spectrometry (ICP-AES), the samples were dissolved using HF. This was done by adding 1 mL of HF (40% in water, Chem-Lab Analytic) and 0.5 mL of aqua regia (3:1 volumetric mixture of concentrated HCl (37%, for analysis, Acros Organics) and concentrated HNO_3 (65%, for analysis, Acros Organics)) to 50 mg of the sample inside of a 100 mL PP bottle. *Caution: Working with HF is extremely dangerous and should only be performed by trained personnel under a fume hood using sufficient personal protection.* After 3 h, the mixture was neutralized using 15 mL of a 30 g/L solution of boric acid (>99%, Fisher Scientific), after which the volume is increased to 100 mL using MQ water. Finally, a further dilution by a factor of 26 is done by the addition of 0.42 M of HNO_3. The elemental analysis was performed using an inductively coupled plasma-atomic emission spectrometer (ICP-AES, PerkinElmer Optima 3300 DV) with signals for Co, Al, Si, and Li at 308.2, 238.2, 251.6, and 670.8 nm, respectively.

2.7. TEM

Transmission electron microscopy (TEM) of the samples was performed with an aberration-corrected JEOL ARM200F Microscope operating at an acceleration voltage of 200 kV and equipped with a cold FEG. Dark-field imaging was performed in scanning TEM (STEM) mode with an annular dark-field (ADF) detector. The samples were prepared via drop-casting a sonicated particle suspension on a holey carbon-coated TEM grid (Cu, 400 mesh, AgarScientific).

2.8. Energy-Dispersive X-ray Spectroscopy (EDX)

EDX analysis of Si, O, and Al in the samples was carried out utilizing a Centurio EDX detector with a solid angle of 0.98 s from a 100 mm^2 detection area.

2.9. Fourier Transform Infrared Spectroscopy

(FTIR) was performed using a Nicolet 6700 Spectrometer equipped with a deuterated triglycine sulfate (DTGS) detector. Prior to analysis, samples were pressed (10^7 Pa) into precisely weighted self-supported wafers of 5−10 mg/cm^2 and degassed *in situ* at 400 °C (5 °C/min heating rate) for 1 h under vacuum (<1 mbar). After degassing, the cell was cooled to 150 °C and a reference spectrum of the material was recorded with an accumulation of 64 scans at a resolution of 2 cm^{-1}. All spectra were compared after normalization to a constant disc mass (∼10 mg/cm^2 of dry catalyst).

2.10. Thermogravimetric Analysis (TGA)

TGA for as-synthesized SSZ-13 was performed on a TA Instruments TGA Q500 instrument under 90 mL/min of O_2. The heating rate was set at 10 °C/min up until 800 °C.

2.11. ^{27}Al and ^{29}Si Solid-State NMR

Solid-state NMR measurements were performed with a Varian Inova spectrometer and an 11.74 T Oxford magnet, thus 500 MHz for protons, using a 4 mm Chemagnetics solids probe. The powdered samples were packed in 4 mm zirconia rotors and spun at 15 kHz at the magic angle. $\pi/2$ acquisition pulse sequence was used for all of the experiments. ^{27}Al spectra were referenced to $Al_2(NO_3)_3$ solution at 0 ppm, while ^{29}Si spectra were referenced to tetrakis(trimethylsilyl)silane (TKS) at −9.9 ppm. Other pulse sequence parameters are listed in Table 1. The acquired signals were zero-filled to 128k points and multiplied with a Gaussian function with 0.015 as the parameter for ^{27}Al and 0.003 for ^{29}Si as apodization steps before performing the Fourier transformation to obtain the spectra.

Table 1. Pulse Sequence Parameters Used in Solid-State NMR for Both ^{27}Al and ^{29}Si Experiments

nucleus	^{27}Al	^{29}Si
NMR frequency (MHz)	130.2	99.3
spectral Window (kHz)	100	30
number of complex points	2000	1600
repetition delay (d1) (s)	1	30
number of scans	2000	1024
pulse width (μs)	3	2.25

2.12. Catalytic Screening (CO_2 Hydrogenation to Olefins)

The catalytic tests were performed in a fixed bed Reactor (PID Eng&Tech) with feed preheating (140 °C). A stainless steel (SS316) reactor is oven-heated with internal thermocontrol. 0.163 g of oxide pellets and 0.153 g of zeolite pellets (125−250 μm) were loaded into the reactor-fitting inert tube with I.D. of 5.8 mm. The activation procedure is using 50 mL of N_2/min during pressure and temperature ramping (10 °C/min to 340 °C and 40 bar). The reactants (N_2, CO_2, H_2 = 1:2:6 molar ratio) were fed to reach space velocities of 18,000 N ml g_{cat}^{-1} h^{-1}. The reaction product was analyzed by online GC every 16 min. The permanent gases (H_2, CO_2, CO, and N_2) were detected by two thermal conductivity detector (TCD) channels, either using He as

https://doi.org/10.1021/jacsau.4c00551
JACS Au 2025, 5, 593−605

a carrier gas or using Ar (for H_2). Hydrocarbons were detected by a flame ionization detector (FID). Equations for calculating the CO_2 conversion (X_{CO2}), reaction selectivity (S_i), yield (S_i), and product space time yield (STY_i) (i = MeOH (methanol), CO (carbon monoxide), DME (dimethyl ether), light olefins (LO), paraffins) can be found in the SI (Section S2).

3. RESULTS

3.1. The Shortcomings of IZC

Figure 2 displays two similar standard IZC syntheses of FAU-to-CHA, only differing in the Al content of the starting FAU. The

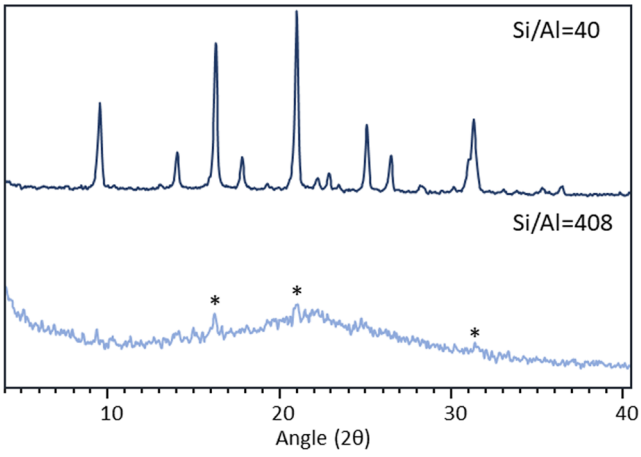

Figure 2. Standard interzeolite conversion of FAU-to-CHA using two FAU mother zeolites with different Si/Al ratios (1 SiO_2: X AlO_2^-: 0.35 TMAdamOH: 17.5 H_2O, 20 h at 160 °C), where $X = \frac{1}{Si/Al}$ displayed in the figure. Stars indicate the presence of CHA reflections in the bottom sample.

batch with a Si/Al ratio of 40 is capable of rapidly forming SSZ-13, and the entire process takes less than 3 h (in agreement with Devos et al.).[17] The system with almost no aluminum (Si/Al = 408) seems to be mostly amorphous after synthesis for 20 h of synthesis. Some crystalline peaks can be observed, however, at 16, 21, and 32°, which are indicative for CHA. This indicates that nucleation has been successful in these conditions, while crystal growth is slowed down. Even after an additional day of synthesis and with the addition of small amounts of alkali cations, which is known to promote crystallization[24] (Figure S2), the synthesis product still mainly consists of amorphous material. While it might be possible to get fully crystalline pure silica CHA by tuning this recipe, it seemed to be much slower than conventional IZC and thus is out of the scope of this research. A rapid, hydroxide-mediated synthesis of high-silica SSZ-13 with an easy, fast, and tunable recipe would be a great asset for making catalysts and adsorbents.[25]

A closer look at the elemental distribution of liquids and solids during a standard IZC (0.35 OH^-/Si), demonstrates that the Al contents of the solid and liquid fractions deviate with respect to each other. Figure 3 shows this distribution at different hydroxide concentrations after 40 min of synthesis. At relatively low concentrations of hydroxide, no significant dissolution has taken place, while if the hydroxide content is increased, incongruent dissolution of silica can be observed. At a higher concentration (0.35) most of the silica is dissolved while aluminum is concentrated in the solid phase (although in absolute terms, Al is a bit more dissolved vs remaining in the solid). Note that due to the total concentration of Si being 40

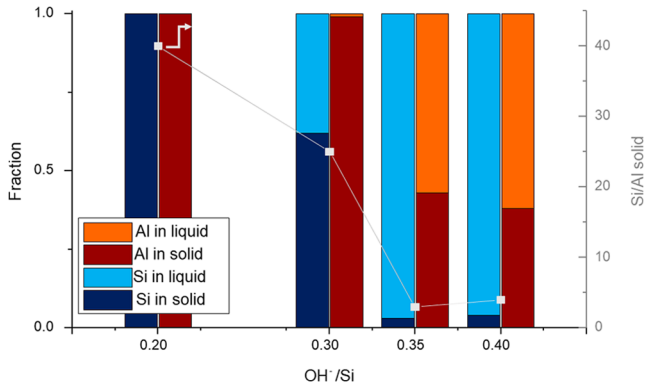

Figure 3. Distribution of Si and Al in the solid and liquid phase and the Si/Al ratio of the solid phase after 40 min of synthesis at 160 °C with the batch composition being 1 SiO_2: 0.025 AlO_2^-: x TmAdamOH: 17.5 H_2O. All experiments were performed using 2.5 g of CBV780. (Line is intended as a guide to the eye. For 0.35: after 45 min).

times higher than that of Al, the Si/Al of the solid phase at this point is around 3−4. As the concentration of hydroxide is increased even further, one would expect full dissolution of the starting source, yet this is not observed. Since hydroxide ions are catalysts for the constant chain of reversible hydrolysis and condensation reactions taking place during synthesis, it also speeds up crystallization.[26] It thus comes to no surprise that after 40 min at 160 °C, the first crystalline peaks can be observed in XRD for hydroxide contents of 0.4 and above (Figure S3, diffractogram for 0.35 can be found elsewhere[17]).

The results in Figure 3 show the sensitivity of the elemental composition of the liquid and solid phases to the hydroxide content (e.g., at OH/Si = 0.3, 64% of the total silica and ∼99% of the total aluminum in the batch reside in the solid phase) and the large discrepancy in Si/Al between both phases after 40 min of standard IZC. This separation of Si and Al in two distinct phases leaves the door open to manipulate the Si/Al ratio of the batch after separation. Selectively removing either the Si-rich liquid phase or some of the Al-rich solid phase (as described in the methods section above) and allowing further synthesis will hereafter be referred to as "split synthesis" (Figure 1). The approach of using the supernatant after dissolution has been previously reported, mainly as a growth solution.[27] Additionally, split synthesis bears some resemblance to the charge density mismatch procedure, where reagents are added after aging or after a short synthesis time. In contrast, the removal of some fraction of the batch contents with the aim of altering the Si/Al ratio after the synthesis has started is entirely novel, especially when combined with IZC. At 40 min of synthesis time, the solids and liquids undergo no observable compositional changes, in contrast to the prior dissolution (0−20 min) and subsequent crystal growth phases (50−90 min), making it an interesting point to manipulate the solid or liquid phase. While theoretically these changes can be performed at any point in the synthesis, at 40 min, solid and liquid compositions are relatively static, making any manipulations more reliable and repeatable.

For the remainder of the manuscript, the following nomenclature will be used to describe specific types of split procedures: a split synthesis in which all solids are removed during the synthesis is hereafter named SPLIT-S, in contrast, when a fraction of the liquids is removed, SPLIT-L(X) will be used, with X the fraction of liquid removed. Finally, in the case that colloidal silica is added during an SPLIT-S procedure, this is written down as SPLIT-S + COL.

https://doi.org/10.1021/jacsau.4c00551
JACS Au 2025, 5, 593−605

3.2. Impact on Batch Composition, Course of the Synthesis, and Product Parameters

Before the effects of a split synthesis on the final product of crystallization can be discussed, an investigation of the batch composition right after the split had to be undertaken. Note that for reasons discussed in Section 3.4, a bit of Li^+ is added. By measuring the elemental composition of the solid and liquid phases after 40 min of synthesis, accompanied by TGA measurements on the solid phase (Figure S4), the mass balance of each batch component in each phase could be calculated. The composition of each phase in wt% is tabulated in Figure 4B

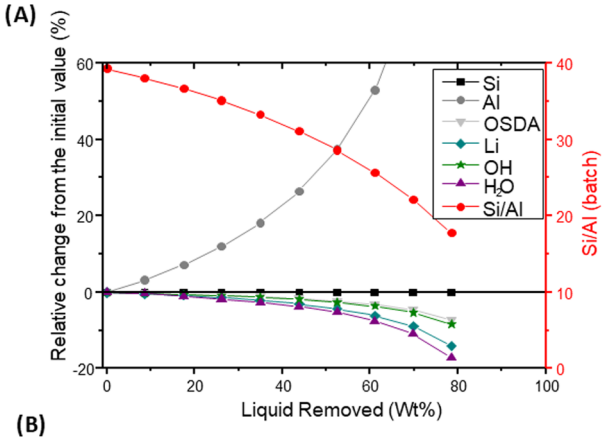

(B)

Fraction	Total weight%	wt% SiO_2	wt% AlO_2	wt% Li^+	wt% $OSDA^+$	wt% H_2O	Si/Al
Total	100.0	13.7	0.3	0.1	13.8	72.1	40.0
solid	0.5	64.4	24.1	0.6	10.9	0.0	2.7
liquid	99.5	13.4	0.2	0.1	13.8	72.5	60.7

Figure 4. (A) Relative change in batch composition for an SPLIT-L system as more of the liquid phase is removed (black) and the Si/Al ratio of the batch is reduced because of this (red). The absolute change in concentration of each batch component can be found in Figure S5. A single, more detailed result for the removal of solids (SPLIT-S) can be found in Table S1. Lines were added as a guide to the eye. (B) Composition of the liquid and solid phases in wt% including Si/Al ratios calculated for a batch composition (at 40 min) before the split of 1 SiO_2 : 0.025 AlO_2^- : 0.06 LiOH : 0.29 TMAdamOH : 17.5 H_2O. The water content of the solid can be neglected.

(note the good agreement with 0.35 OH^-/Si point of Figure 3 without Li^+). When subsequently, a certain amount of solid or liquid is removed from the reactor during the split synthesis, the resulting batch composition can be estimated by subtracting a known amount of each batch component in the removed phase from the starting amount. By plotting out the wt% of liquid removed from the batch (vs the entire weight of synthesis medium) versus the change of a certain batch component with respect to the initial state, the impact removing liquid has on the remaining batch composition (relative to no removal) can be visualized (Figure 4A, the absolute change in terms of molar batch concentrations can be found in Figure S5).

Figure 4A shows that removing progressively more of the Si-rich liquid (SPLIT-L) still allows most of the batch components to stay within 20% of their original value (in our selected batch composition), although with a slight decrease. Only the Al concentration shows a drastic increase as the amount of liquid removed reaches 80% of the total batch weight. This increase in Al content translates itself in a decrease in Si/Al in the synthesis liquor (red line, Figure 4A) which is easy to rationalize as Al is the only element that is concentrated in the solid phase (Figure 4B) and thus the only one experiencing large influences from changing the solid/liquid ratio inside of the autoclave. Additionally, it must be noted that since an autoclave with the same volume was used to perform the second stage of synthesis, and a fraction of the synthesis medium is removed from reaction, the overhead volume of the reactor increases, leading to a relatively larger fraction of water lost due to evaporation than depicted in Figure 4A. The relative inertness of the batch composition means that we have an easy way of changing the Si/Al ratio of an IZC after dissolution of the mother zeolite is complete without having a significant impact on any other factors (not only concentration but also mixing, dissolution, etc.). Effects of this procedure on the synthesis and their outcome will be discussed next.

Figure 5 displays a crystallization curve of a synthesis in which all of the solid phase has been removed after 40 min of synthesis

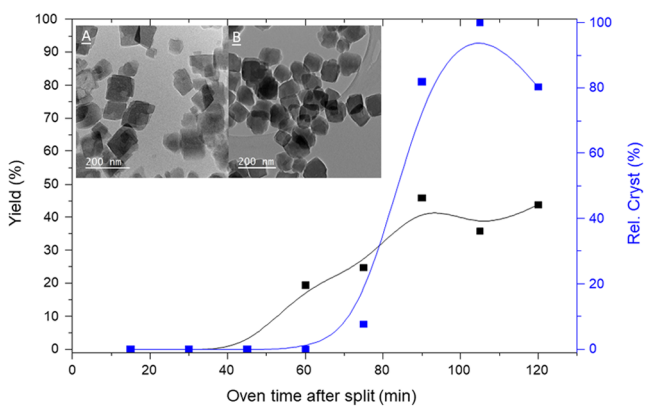

Figure 5. Yield and relative crystallinity of an SPLIT-S synthesis (split after 40 min at 160 °C). Starting batch composition is 1 SiO_2 : 0.025 AlO_2^- : 0.06 LiOH : 0.29 TMAdamOH :17.5 H_2O. These experiments were performed using 2.5 g of CBV780. Inset A: TEM images of a split synthesis in which the solids are removed (40 min + 20 h at 160 °C) Inset B: A standard IZC without a split. Both methods result in similar crystal shapes and morphologies. More info can be found in the SI. Bezier-spline curves are added as guides to the eye. Inset B is reproduced from ref 15. Copyright 2023 American Chemical Society.

(SPLIT-S, for diffractograms and pictures, see Figures S6 and S7). First, it can be noted that the yield of the SPLIT-S synthesis (which lies around 45%) is slightly lower than the 55−60% obtained in similar syntheses.[8,15,17] This can easily be explained by the fact that we calculated the yield based on the initial amount of zeolite which was dissolved in the hydroxide solution and not on the amount of Si and Al present at the time of split. A more in-depth discussion on this can be found in the Supporting Information (Section S1 and Figure S1). When comparing the duration of the crystallization (stage III of IZC[17]) after an SPLIT-S at 40 min with that of a standard IZC[15,17] with a similar recipe, one can see that the procedure is only marginally slower when performing a split synthesis in which the solids are discarded (40 min until split +90−100 min of crystallization = 130−140 min total) versus when performing a standard IZC (approximately 120 min) using a similar recipe, albeit with a higher Si/Al ratio (35 vs 70). This is surprising for two reasons.

(1) Heat transfer limitations will lead to the autoclave possibly not reaching thermal equilibrium in the 40 min synthesis time before the split.[28] And since the synthesis is

https://doi.org/10.1021/jacsau.4c00551
JACS Au 2025, 5, 593−605

cooled down after 40 min, the synthesis mixture experiences a heat up period which is doubled in time compared to the standard IZC process. Nucleation and crystal growth speed are affected by the temperature of the synthesis,[29,30] so it would be expected that the SPLIT-S synthesis would be slower. This not being the case provides some evidence toward the idea that the biggest energy barriers for the IZC of FAU-to-CHA (i.e., dissolution and nucleation[29]) have already been overcome before the split. Or, at the least, that nucleation is not the rate-limiting step, which could again be explained by the fact that the energetic barrier for nucleation is inversely related to the degree of supersaturation.[31,32]

(2) Removal of the solid phase prevents them to act as nucleation sites for further zeolite formation. Surfaces provided by the presence of the solid phase can lower the energetic barrier of nucleation toward a target zeolite.[16,33] It would thus be expected that the removal of these (heterogeneous) nucleation sites will slow down the entire synthesis. However, it does seem likely that the incomplete separation by centrifugation and reuse of the original PTFE liner leads to small amounts of solid phase still being present in the synthesis solution. Additionally, Cundy and Cox stated that filtration or centrifugation of reaction media is insufficient for the removal of all amorphous "solids" from a reaction media as there will always be undetectable colloidal species being transferred which behave in a similar way to the solid phase.[2] Okubo and co-workers indicated the promotional effect of stopping a synthesis and doing intermediate stirring on the crystallization of target zeolites.[34] Having a look at the insets A and B in Figure 5 which compares a SPLIT-S synthesis (A) with an identical batch which did not undergo a split procedure (B), one can see the similarity between particle morphology and size (~200 nm, cubic). Additional TEM pictures and particle size distributions can be found in SI (Figures S14 and S16). These small crystals are typical for seeded syntheses (which IZC essentially is) and are a result of the vast amount of nucleation sites present during synthesis.[35] The similarity between inset A and B gives some evidence toward the idea that the Al-rich solids, which were removed from the reaction mixture, are actually not the initial site of nucleation and that their main role is to act as a buffer for Si and Al atoms during the synthesis.[36]

These two considerations lead to the possible conclusion that nuclei or prenucleation clusters are probably already present in the liquid as dissolved oligomers or in small colloids after 40 min of synthesis at the moment the split is performed.

3.3. Split Synthesis as a Method for Control over Product Si/Al

Now that the split procedure has been established as an interesting procedure for controlling the Al content of a zeolite (and the synthesis mixtures), we will go more in depth on what are the operational ranges of this system. After separation of the two fractions, either the alumina-rich solid is removed (SPLIT-S) to increase the Si/Al ratio of the batch or (part of) the Si-rich liquid is removed (SPLIT-L) to decrease the Si/Al ratio of the mixture. Additionally, we investigated whether the addition of amorphous silica sources at the moment the split takes place (SPLIT-S + COL) helps to increase the Si/Al even more. This was done for both FAU-to-MFI and FAU-to-CHA IZC systems. While the results of MFI can be found in the SI, they are discussed below for CHA.

Figure 6 shows the Si/Al ratio of the SSZ-13 zeolite made by an SPLIT-L synthesis where progressively larger fractions of

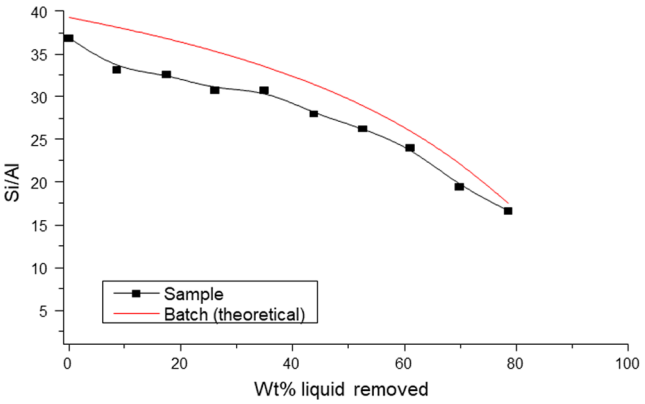

Figure 6. Si/Al ratio of the zeolite vs the Si/Al ratio of the resulting CHA zeolite for a series of SPLIT-L syntheses with starting batch composition of 1 SiO_2 : 0.025 AlO_2^- : 0.06 LiOH : 0.29 TMAdamOH : 17.5 H_2O. The red line is the theoretical Si/Al upon removal as depicted in Figure 4.

liquid are removed from the synthesis mixture. As can be seen, the Si/Al ratio of the product zeolite quite closely follows the Si/Al ratio of the batch, with the former only being slightly lower than the Si/Al ratio of the latter. This indicates that the incorporation of Al is more complete than that of Si when crystallizing CHA zeolites. This result, together with the absence of impurities in the diffractogram (Figure S8), the large pore volumes still observed even for samples made with 60 wt % liquid removal (Table 2), and the absence of octahedral EFAL

Table 2. Resulting Properties of 1 IZC and 2 Split Syntheses Where a Certain Fraction Is Removed

sample	Si/Al[a]	DCC (Co/Al)[a]	Li/Al[a]	micropore volume (cm^3/g)[b]	corrected yield (%)
IZC	37	0.45	0.68	0.30	59
SPLIT-S	65	0.61	/	0.32	47
SPLIT-L(60)	24	0.41	0.47	0.31	67

[a]measured by ICP. [b]measured by N_2 physisorption.

species (Figure S12) shows the SPLIT-L(60) crystallization keeps delivering pure crystalline CHA in the more aluminous conditions. A comparison is made between a standard IZC from FAU to CHA containing Li (previous work, no split) and an SPLIT-L(60) synthesis and is displayed in Table 2. It shows an increase in the corrected yield (in contrast to the actual yield; more information about the corrected yield can be found in Section S1) as more Si-rich liquid is removed at the time of the split. This is expected for two reasons: (1) Al (-rich zeolites) are less soluble in hydroxide medium than more siliceous ones and (2) CHA is known to be energetically more stable when crystallizing in Al-rich conditions.[18] In contrast, the decrease in batch Si/Al for MFI (ZSM-5) upon liquid removal is indicative of an increasingly difficult crystallization stage (Figure S20).

For MFI, a decrease is observed in the pore volume of the end product, indicating an incomplete conversion of the starting material into MFI, confirming that MFI has a lower stability

https://doi.org/10.1021/jacsau.4c00551
JACS Au 2025, 5, 593−605

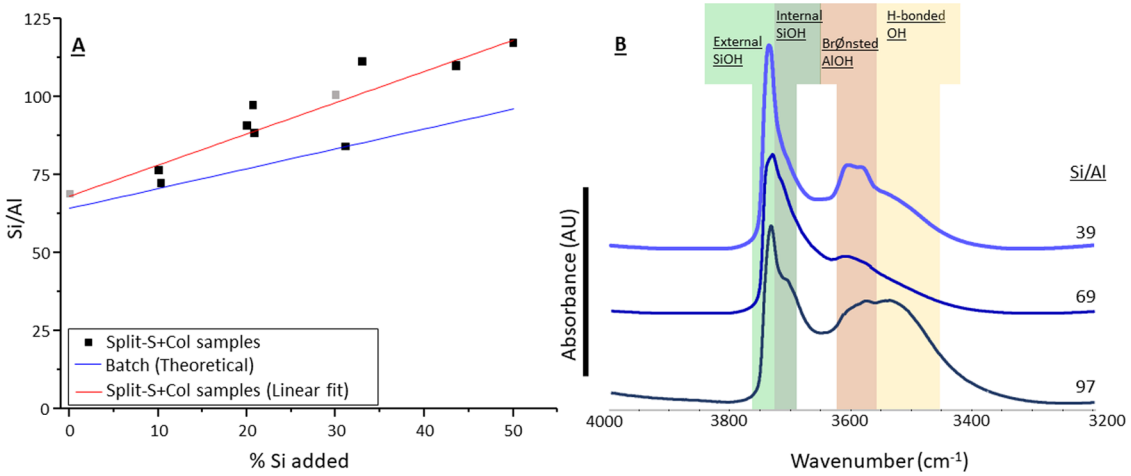

Figure 7. (A) Si/Al ratio of the batch (blue line) and the formed SSZ-13 zeolite (red line) after a SPLIT-S + COL procedure, starting from a batch composition of 1 SiO_2 : 0.025 AlO_2^- : 0.35 TMAdamOH : 17.5 H_2O. The red curve is a linear fit of the data with an R^2 = 0.81. The blue curve is the estimated of the batch Si/Al based on calculations and a single experimental point (composition after split at 40 min). The % of Si added is calculated versus the amount present in the batch after split. The gray squares represent samples that are also displayed in (B). (B) FTIR spectra of several SSZ-13 zeolites synthesized by IZC (39) or split synthesis (69 + 97), gray cubes in (A). Band assignment was performed according to Bordiga et al.[39].

when forming in Al-rich conditions.[8,18,37] The formation of more Al-rich SSZ-13 zeolites (as seen in Figure 6) is not challenging and has been achieved countless times before in nonsplit syntheses, but more interesting here is the effect this procedure has on the resulting Al distribution of the SSZ-13 zeolite (see Section 3.4).

It would in fact be more interesting to increase the range of Si/Al ratios of the SSZ-13 accessible from hydroxide media to Si/Al = 60−250 for both catalysis and adsorption. The removal of the Al-rich solid fraction at the split time already achieves this goal practically as the Si/Al ratio of the product is 65 (quite remarkable for CHA in OH-media). This is already substantially higher than the Si/Al of 35 obtained with a standard IZC of the same recipe, without having a grave impact on the overall oven time (discussed before in Figure 5), phase selectivity, or micropore volume (Table 2). Similar results were obtained for a TPAOH-containing synthesis which forms MFI (Figure S9), these results are less surprising as MFI is known to easily crystallize in silica-rich media.[18] A short investigation on the effect of split time on the SPLIT-S synthesis of SSZ-13 was included in SI (Figure S10); however, aside from the yield, the impact appeared limited.

To expand the range even further, an attempt was made to add (colloidal) silica at the moment of the split after the Al-rich solid phase is removed (SPLIT-S + COL). Figure 7 shows the validity of this strategy as an increase of the Si/Al ratio is found in the product zeolite when more colloidal silica is added to the batch, without a reduction in pore volume (Figure S11) indicating the crystallization of CHA is not influenced and no amorphous nonporous fractions are formed. The Si/Al ratio of the formed zeolite follows that of the batch composition quite closely. It is important to note that the addition of colloidal silica to the mixture alters the batch composition, since it is normalized to the amount of Si inside of the mixture, and the most important impact of this effect is the decrease of the OSDA(OH)/Si ratio. This has two important consequences; it will naturally increase the Si/Al ratio of the formed zeolite as silica is less soluble in less alkaline conditions,[38] explaining why the batch Si/Al and zeolite Si/Al increase with a different slope in Figure 7. Additionally, it will (presumably) slow the crystallization process. Interesting to note is the effect this increase in Si/Al has on the silanol and aluminol content of the final zeolites as measured by FTIR (Figure 7B).[39] Two trends are visible in the FTIR spectra; first, as the Si/Al increases, the Al−OH signal decreases in intensity, confirming a reduction in the amount of Al inside of the framework. An increase in the population of internal SiOH bonds can also be observed as the Si/Al is increased, due to the necessity of charge compensating silanols[40] for the charge of the template as there is not enough Al present to fulfill this role. Finally, a large contribution of H-bonded OH groups can be found in all samples, signifying that despite the high Si/Al, these frameworks are still highly defect-rich and hydrophilic. When observing the ^{29}Si MAS NMR results displayed in Supporting Information (Figures S12 and S13), three signals can be distinguished. The signals for Q^4(0Al) and Q^4(1Al) are located at −111 ppm and −105 ppm, respectively.[41] The relative proximity to the Q^4(1Al) signal at −105 ppm but the small shift downfield, together with the observation that this signal hardly changes as the Si/Al of the crystal changes, seem to indicate that the signal at −102 ppm is caused by Q^3 (3Si, 1OH) species.[41] This conclusion is strengthened by the fact that excluding this signal from the calculation of Si/Al through Engelhardt's formula[41] gives results that are much closer to the ones measured in ICP. Interestingly, the increase in silanols obtained from FTIR, was not observed by ^{29}Si NMR.

Next, TEM(-EDX) was utilized to check the elemental distribution and morphology of an SPLIT-S + COL sample (Figures S12, S13 and S16). First, when comparing the morphology of four samples (standard IZC, SPLIT-S, SPLIT-L(80), and SPLIT-S + COL), it can be noted that the morphology and sizing of the zeolites are quite similar (100−200 nm), only showing a slight increase in crystal size as higher Si/Al ratios are reached. Morphology-wise, all crystals have a cubic appearance with some rugged edges, especially in the sample with the lowest Si/Al, individual crystallites can be observed, pointing to a growth mechanism dominated by growth by particle attachment.[36] The highest Si/Al ratio zeolite (SPLIT-S + COL) shows (a bit) smoother edges, probably due to the slow supply of silica monomers from colloidal silica, which leads to classical crystal growth at the end of the synthesis. Al

https://doi.org/10.1021/jacsau.4c00551
JACS Au 2025, 5, 593−605

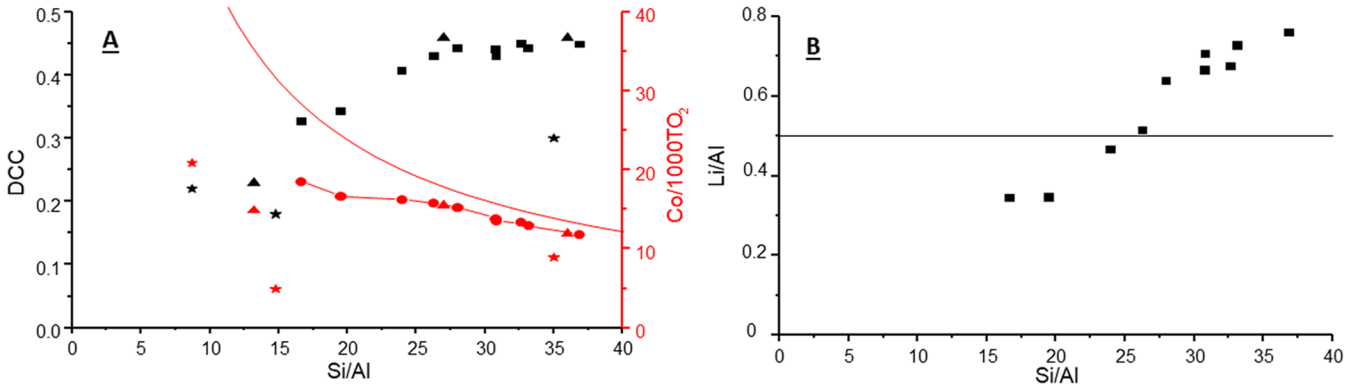

Figure 8. (A) DCC (Co/Al)(■) and Co/1000TO_2 (red circle solid) as a function of the synthesis mixture Si/Al after SPLIT-L procedure (1 day at 160 °C, Batch Comp: 1 SiO_2 : 0.025 AlO_2^- : 0.06 LiOH : 0.29 TMAdamOH : 17.5 H_2O), also for standard IZC's with different starting Si/Al ((Co/1000TO_2: red triangle up solid, DCC: ▲), i.e., from FAU with Si/Al 40, 30, and 15), and literature values (Co/1000TO_2: red star solid, DCC: ★).[12,13,17] The red line represents the theoretical maximum for Co/1000TO_2. (B) Li/Al value as a function of the DCC for the split samples; the solid line indicates a Li/Al level of 0.5.

zoning would be expected in these cases, as the liquid phase, where nucleation starts, is relatively more aluminous than the colloidal silica, and the solution is already supersaturated, inhibiting any further dissolution of the silica before hydroxide is released by condensation of soluble Si species. However, TEM-EDX shows no zoning (Al or Si) inside of the zeolite crystals (Figure S15). This is probably caused by the crystal growth being heavily dominated by particle attachment, and while Al zoning inside of the individual crystallites of a particle would thus be possible, this would be difficult to detect as the zones of high and low Al content would overlap, resulting in an averaged Al distribution. Additionally, Al is known to be mobile in zeolite synthesis;[8,42,43] hence, a redistribution of Al does not seem impossible.

Finally, to test the limits of this technique in reaching higher Si/Al ratios, an attempt was made by reducing the OH^- content to 0.3 of the initial batch mixture before the SPLIT-S + COL synthesis (with 30 wt % of added colloidal silica). As discussed in Section 3.1, the reduction of the OH^- content of the batch will result in a more siliceous liquid and a larger retention of Si, and especially Al, in the solid phase. As a result, the Si/Al of the liquid phase was thus higher. A crystallization time postsplit of 20 h at 160 °C yielded an SSZ-13 zeolite with a Si/Al ratio of ∼180. The zeolite was still very crystalline (XRD) and open (0.34 cm^3/g micropore volume, Figure S17), indicating that the limits of this system might be pure siliceous CHA (in fast hydroxide conditions!). A calculation of the particle size distribution of a similar sample (SPLIT-S + COL starting from OH/SiO_2 = 0.32 with the addition of 30% colloidal silica at split, Si/Al = 110) shows this procedure produces relatively larger particles (approximately 160 vs 120 nm, Figure S18).

3.4. Adsorption of Divalent Cobalt: A Peak into Aluminum Distribution

Given that Si/Al control over CHA can be steered via split syntheses (all three variants) in both directions, a closer look at the Al distribution of the synthesized CHA- and MFI-type zeolites is warranted. The divalent cation capacity (DCC), measured as a simple Co/Al ratio after an aqueous Co exchange at mild conditions, is often used as a proxy for the presence or absence of proximate Al sites.[10] These are 2 Al atoms which are close enough in proximity (AlO(SiO)nAlO with n = 1 or 2) and in an energetically beneficial location to take up Co^{2+} ions[10,44] from the liquid phase. While this method has been used successfully in the past and clearly correlates to activity in some catalytic reactions such as the dehydration of methanol,[45] one still has to exert caution during the analysis as there can be multiple other adsorption sites for Co^{2+} cations such as amorphous fractions or silanol nests.[8] Additionally, thermal vibrations during UV−vis measurements make it impossible to assign specific sites to the adsorbed Co^{2+}, which, nonetheless, is a common practice in the field.[46] Here we thus intend to use the method as a broader analytical tool, i.e., not just for determining the amount of paired Al but also for identifying other possible adsorption sites.

Figure 8a shows the cobalt uptake (Co/Al and Co/1000TO_2 in red) of the SPLIT-L samples already displayed in Figure 6. When analyzing the Co uptake of a sample, one must be careful, as the DCC is a metric based on both the Co uptake and the amount of Al present in the framework. Hence, the Co/1000TO_2 is a better metric to study the absolute amount of Co taken up by the framework. The Co/1000TO_2 has a theoretical upper limit (displayed by the continuous red line in Figure 8) if one assumes the only species for Co uptake are two proximate Al sites. In these synthesis trials, Li was added as it was previously found to have a positive impact on the DCC in both IZC and conventional syntheses;[12,15] additionally, when Li was omitted from the synthesis, no considerable changes were observed in Si/Al, only in the DCC (Figures S21 and S22). When looking at the DCC in Figure 8a, both the IZC syntheses with lower Si/Al starting materials and the SPLIT-L syntheses follow a similar trend. The DCC is stable close to its maximum (of 0.5) until a Si/Al of 24 is reached, whereafter a linear decrease in DCC takes place for lower Si/Al syntheses. The Co/1000TO_2 vs Si/Al trend shows a more linear trend in comparison to the DCC (Figure 8), slowly moving away from the theoretical plot as the Si/Al value is lowered. The highest Co/1000TO_2 reached by SPLIT-L(80) syntheses is approximately 18 with the DCC at 0.33. This peculiar decrease in DCC can be explained by a decrease in the Li/Al of the product zeolites under a value of 0.5 (Figure 8b). For a pair of proximate Al to be stabilized from synthesis, there is a need for two charges, conventionally, one of these charges is provided by the OSDA and the other by the presence of an alkali metal (Li in our case).[12−1314,43] It thus comes as no surprise that when decreasing the Li/Al ratio below the threshold of 0.5, the DCC starts to drop suddenly. Surprisingly, the course of the absolute amount of Li

https://doi.org/10.1021/jacsau.4c00551
JACS Au 2025, 5, 593−605

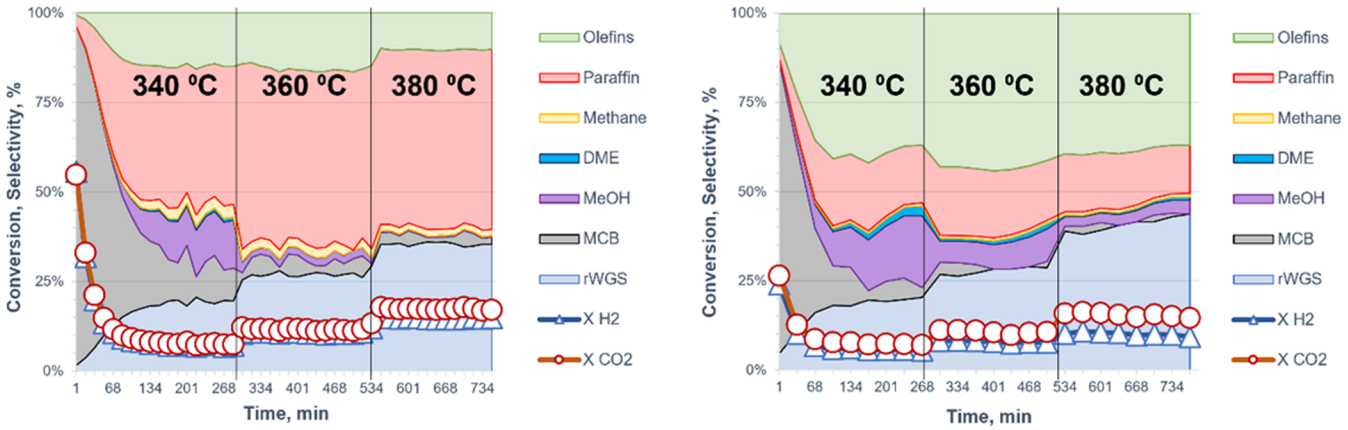

Figure 9. Conversion of CO_2 and H_2 reactants (circles) and reaction selectivity for a ZnZrOx-zeolite tandem for CO_2 hydrogenation to olefins, using SSZ-13 with Si/Al ratios of 15 (left) and 111 (right). The high silica (right) is synthesized by SPLIT-S + COL synthesis (see Section 3.3, for XRD of the calcined material, see Figure S24). Reaction selectivity demonstrates selectivity to predominantly hydrocarbons (paraffins and light olefins), and some CO (rWGS reaction), after an initial reaction time of precoking, quantified as missing carbon balance (MCB; see the SI).

encapsulated in the daughter zeolite (Li/1000TO_2, Figure S19) stays relatively constant for a wide range of Si/Al ratios, only increasing for MFI as the crystallization for MFI is incomplete at lower Si/Al ratios, giving rise to low crystallinity and small pore volume (Figure S20). Since the Li/Si ratio in the reactor stays relatively constant during this SPLIT-L procedure as more liquid is removed (Figure 4A), this would indicate that the total uptake of lithium during a zeolite synthesis is only dependent on the initial amount, which is present during the crystallization, and not on the Si/Al ratio of the formed daughter zeolite. Additionally, this implies that, since the OSDA content also nearly stays constant (gray inverted triangles in Figure 4A), the total amount of charge compensating groups present in the framework (i.e., defects + Al) also stays constant.

When looking at the DCC versus Si/Al during SPLIT-L synthesis of different systems (than the FAU to CHA containing Li), some interesting observations can be made (Figure S22). For an FAU to CHA SPLIT-L synthesis not containing any Li, with a similar initial composition as the one investigated by Devos et al.,[47] it can be seen that due to the absence of Li, the DCC of the sample which underwent no SPLIT-L synthesis has a lower DCC overall due to the absence of Li. Additionally, there is a much larger variation in the DCC values obtained in this sample, in comparison to the Li containing SPLIT-L, probably stemming from the mobility of Al in the absence of Alkali cations and the absence of a strong thermodynamic drive for these Al pairs to form in the first place. Finally, the DCC vs Si/Al of the MFI(Li) system seems to stay constant, even though the crystallinity of the framework decreases drastically toward lower Si/Al values (Figure S20).

A final observation regarding the DCC can be made when looking at the SSZ-13 zeolite in which the solid has been removed (with a final Si/Al of 65). Table 2 shows that the DCC surpasses the theoretical maximum of 0.5 and reaches a value of 0.61. This indicates that proximate Al sites are not the only ones stabilizing Co^{2+} cations. Since the zeolite has an open structure as can be seen from N_2 and there are no peculiar fractions present in TEM, we have to conclude that there are other zeolite-associated sites responsible for this uptake of Co^{2+}. The prime suspects for this would be silanol defects; however, other sites such as framework-associated Al or the outer surface might also be potential Co^{2+} adsorption sites.

3.5. Application of High-Silica SSZ-13 in CO_2 Hydrogenation to Olefins

To show the relevance of the synthesized samples and the usefulness of uniquely high Si/Al made in hydroxide media, a few high-silica SSZ-13 were subjected to tandem CO_2 hydrogenation to olefins (cf. the experimental procedure). This tandem reaction is under intense investigation and offers certain benefits versus single CO_2-to-methanol followed by methanol-to-olefins (MTO).[48] SSZ-13 with a different Si/Al was (particle) mixed with ZnZrOx, which catalyzes the hydrogenation of CO_2 to methanol. This methanol then reacts further to olefins inside the pores of the SSZ-13 zeolite, along a type of MTO chemistry but in the presence of high pressures of CO_2 and hydrogen. The latter is beneficial for the catalyst lifetime.[49,50] In Figure 9, the performance of SSZ-13 prepared by SPLIT-S + COL synthesis (Si/Al_{ICP} = 111) is compared with an Al-rich SSZ-13 prepared by direct IZC synthesis (Si/Al = 15, synthesized according to the literature[51]). Similar CO_2 conversions are observed along with a large difference in product distribution. After the initial precoking in zeolites, quantified via the missing carbon balance (MCB, see Section S2, Supporting Information), a significant difference in hydrocarbon product distribution is found. Olefin to paraffin ratios (O/P) increases from 0.5 in the aluminous sample (Si/Al = 15) to 2.6 in the SPLIT-S + COL sample (Si/Al = 111) during reaction at 380 °C. Likely this is due to inhibition of secondary hydrogenation, occurring on less numerous acidic Al.[52] Since olefins are the desired product, the latter represents a significant amelioration in CO_2-to-olefins performance, induced by the synthesis procedure of high-silica SSZ-13 obtained by SPLIT-S + COL modification. Note however that the zeolite function is susceptible to deactivation; methanol conversion ceases within 1−2 days (Figure S23). Adequate adaptation of pretreatment and reaction conditions (temperature, pressure, etc.) can be used to maximize the long-term stability, given the complex and dynamic MTO chemistry occurring in zeolites.[53] Overall, the system with an SPLIT-S + COL high-silica CHA has a very high maximal reaction yield of olefins of 6% (66% yield in the hydrocarbon fraction), reaching olefin productivities (space time yields) of 10 mol carbon h^{-1} kg_{cat}^{-1}. Moreover, using a high-silica CHA integrated in tandem with ZnZrOx is also beneficial for the maintenance of the long-term stability of olefin product yields. While the data set in Figure 9 is rather limited,

https://doi.org/10.1021/jacsau.4c00551
JACS Au 2025, 5, 593−605

Chen et al. showed constant product distributions at very high TOS (>100 h) for their high-silica SSZ-13 (Si/Al_{ICP} = 34).[54] Their study demonstrated a similar shift in product distribution from paraffins to olefins due to lower Al contents. However, due to conventional synthesis methodologies, high framework Si/Al (>60) could not be created. In contrast to traditional methods, our SPLIT-S + COL synthesis methodology achieves high-silica CHA zeolites synthesized in hydroxide medium. Thanks to their high Si/Al ratio and small sizes in contrast to 1−10 μm big crystals that would be formed from an F^- medium, the split methodology holds promise for excellent olefin product selectivity and a relatively long lifetime in CO_2 hydrogenation catalysis.

4. DISCUSSION

The need for flexible, cheap, and easy zeolite synthesis recipes has never been higher, and while interzeolite conversion seems to be an ideal method for exerting fine control over zeolite (Al distribution, morphology, etc.) and synthesis properties (speed, viscosity, etc.), there are boundaries to what can be achieved. As was shown by the IZC of pure silica FAU zeolite to CHA in Figure 2 and by extension Figure S2, nucleation seems possible in these highly siliceous conditions and it might even be possible to fully crystallize SSZ-13 in these conditions by exchanging part of the template by Li, which is known to be an accelerant for the crystallization of SSZ-13.[15,55] However, this does come at the cost of the speed of crystallization, and (as was the case for the Li-free synthesis) it might be that the formation of other competing phases takes place during the synthesis. A recent publication by Liu and co-workers achieved the formation of pure Si SSZ-13 by the conversion of pure silica SOD.[23] They appointed this successful transformation to the heteroepitaxial growth of CHA crystals on the surface of the dissolving SOD, thus lowering the energy barrier for nucleation. It seems unlikely a similar mechanism of nucleation is present here, since the reaction medium is more alkaline than the one used by Liu et al. (OH/SiO_2 = 0.2 vs 0.35 here) and more aluminous (and thus less soluble in hydroxide media) FAU zeolites have been observed to be almost fully solubilized in similar conditions to ours.[47] Thus, the only time a viable surface for nucleation is present is during the dissolution of the starting zeolite; however, it is highly unlikely that these nuclei would survive for the period necessary to initiate crystal growth. A mechanism in which nucleation takes place from the liquid (or a colloidal suspended) phase thus seems more likely in the pure silica FAU-to-CHA IZC investigated here. Furthermore, it is clear that the presence of some Al accelerates the synthesis of CHA zeolites through IZC in this work (as well as in the literature[16,56]). Using split synthesis allows for the nucleation and growth to take place under more beneficial conditions, after which the synthesis conditions are altered to obtain useful zeolite properties (e.g., high Si/Al ratio) that otherwise would be difficult to obtain. Split synthesis thus allows for the formation of zeolite products outside of their usual range of stability and with properties not easily combined.[18,57]

The fact that split synthesis is capable of synthesizing zeolites with small crystals over such a broad range of Si/Al ratios (CHA: 14−70 (180 with the addition of colloidal silica) MFI: 30−80) in a rapid manner, starting from a single batch composition and an easy and reproducible synthesis, is a great feat and can be attributed to the kinetic nature of interzeolite conversion. Due to the high lability of high-silica FAU in hydroxide medium, the dissolution is very rapid.[58] As a consequence, high supersaturation is reached in the liquid phase.[16] This provides a rather large thermodynamic driving force toward the condensation of solubilized silica into a solid phase, as has been shown by the rapid nucleation and crystal growth[35,59] observed in similar IZC systems.[16] Due to this high thermodynamic driving force and subsequent rapid crystal growth, we pose that the first phase to form viable nuclei will thus be the dominant phase in the product. The addition of a second silica source right before crystal growth takes place during the split introduces some additional variation to the synthesis (which is already on a nucleated track). Since the supernatant is already supersaturated after the dissolution of the FAU zeolite and the pH of the synthesis medium is rather low at this point (∼11.6)[15] we do not expect the colloidal silica to dissolve completely initially, only dissolving completely as the crystal growth has started and OH^- is being released because of this, effectively acting as a reservoir.

We predict that split syntheses as has been displayed here for two relatively easy-to-synthesize frameworks (CHA and MFI) have wider applications in different syntheses conditions. While the use of supernatant solutions has been displayed before in zeolite synthesis, these solutions were often made by utilizing more conventional source materials, which are either relatively slow to dissolve, or as has been shown by Chen et al. rapidly condense to form more inert structures.[60] As a result, supersaturation will never be this high, as is the case here when using a high-silica FAU zeolite as a starting source, causing the thermodynamic drive for crystallization to be lowered. Second, to the best of our knowledge, this is the first time that the dissolution conditions that produce the supernatant have been actively tuned to change the outcomes of the final product, introducing novelty into the procedure.

Finally, it does need to be mentioned that exact and reproducible control over the Si/Al ratio is only feasible for systems that display a period in which a steady-state equilibrium is observed at a certain time, as systems that display major changes over short times will be difficult to stop at the same progress in their synthesis consistently. Despite this, the principles on which split syntheses are built seem to be general and applicable to any interzeolite conversion where there is no formation of a viscous gel phase (where liquid removal is impossible). This leads us to believe that split syntheses might be beneficial for the bottom-up tuning of the Si/Al ratios of zeolites which are stuck in a relatively narrow region of Si/Al (e.g., AEI, AFX, LEV, etc.),[1] if the conditions are well chosen.

5. CONCLUSIONS

In this work, split synthesis was introduced as a viable alternative and rapid synthesis for a few zeolite topologies with a wide range of compositions (Si/Al 15−180) in hydroxide medium by starting from identical batch compositions. It was discovered that by stopping a standard FAU-to-CHA IZC synthesis after incomplete dissolution of the starting source, it is possible to exploit the inhomogeneous distribution of elements (Si and Al) between the solid and liquid phases to steer the elemental composition, and thus a range of other properties (catalysis, acidity,...), of the final product. By removing a fraction of the Si-rich liquid (SPLIT-L), the Si/Al ratio of the resulting CHA zeolite decreased, while retaining a small particle size and, up to certain (decreasing) Si/Al, a high divalent cation capacity. It was shown that the concentration of Li taken up by the zeolite is the limiting factor in maintaining a high divalent cation capacity. Alternatively, by removal of the Al-rich solid (SPLIT-S, with or without the addition of additional silica), it was possible to

https://doi.org/10.1021/jacsau.4c00551
JACS Au 2025, 5, 593−605

increase the Si/Al ratio of hydroxide media CHA to new heights (Si/Al ~ 180) in both a rapid and practical method. This yields CHA zeolites with few acid sites and small particles, opposed to those highly siliceous but very large crystal samples from F^--mediated synthesis in the art. These zeolites, when mixed with ZnZrOx showed great potential as a catalyst for the conversion of CO_2 and hydrogen to olefins, evident from high olefin selectivity and a competitive lifetime. Additional experiments performed on the IZC of FAU-to-MFI showed that split syntheses are quite generally applicable and thus flexible tools to tune the elemental composition of a target zeolite. We predict that further exploitation of this technique could expand the elemental (target Si/Al) range of other difficult-to-synthesize zeolites.

■ ASSOCIATED CONTENT

Supporting Information

The Supporting Information is available free of charge at https://pubs.acs.org/doi/10.1021/jacsau.4c00551.

Photographs, nitrogen physisorption isotherms, diffractograms, and an additional section on yield calculation for the zeolite synthesis and the CO_2 conversion (PDF)

■ AUTHOR INFORMATION

Corresponding Author

Michiel Dusselier − *Center for Sustainable Catalysis and Engineering (CSCE), KU Leuven, B-3001 Leuven, Belgium;* orcid.org/0000-0002-3074-2318; Email: michiel.dusselier@kuleuven.be

Authors

Sven Robijns − *Center for Sustainable Catalysis and Engineering (CSCE), KU Leuven, B-3001 Leuven, Belgium;* orcid.org/0000-0001-9229-1578

Julien Devos − *Center for Sustainable Catalysis and Engineering (CSCE), KU Leuven, B-3001 Leuven, Belgium;* orcid.org/0000-0002-2254-9016

Beatrice Baeckelmans − *Center for Sustainable Catalysis and Engineering (CSCE), KU Leuven, B-3001 Leuven, Belgium*

Tom De Frene − *Center for Sustainable Catalysis and Engineering (CSCE), KU Leuven, B-3001 Leuven, Belgium;* orcid.org/0000-0001-6768-4732

Mostafa Torka Beydokhti − *Center for Sustainable Catalysis and Engineering (CSCE), KU Leuven, B-3001 Leuven, Belgium*

Rodrigo de Oliveira-Silva − *Centre for Membrane Separations, Adsorption, Catalysis and Spectroscopy for Sustainable Solutions (cMACS), KU Leuven, B-3001 Leuven, Belgium;* orcid.org/0000-0003-3903-2678

Niels De Witte − *Department of Chemical Engineering, Vrije Universiteit Brussel (VUB), B-1050 Brussels, Belgium;* orcid.org/0000-0002-3541-1382

Dimitrios Sakellariou − *Centre for Membrane Separations, Adsorption, Catalysis and Spectroscopy for Sustainable Solutions (cMACS), KU Leuven, B-3001 Leuven, Belgium;* orcid.org/0000-0001-7424-5543

Tom R. C. Van Assche − *Department of Chemical Engineering, Vrije Universiteit Brussel (VUB), B-1050 Brussels, Belgium;* orcid.org/0000-0002-0739-5688

Complete contact information is available at: https://pubs.acs.org/10.1021/jacsau.4c00551

Notes

The authors declare no competing financial interest.

■ ACKNOWLEDGMENTS

S.R., N.D.W., T.R.C.V.A., and M.D. thank the Research Foundation Flanders (FWO Vlaanderen) for funding (Grants G085220N and G0A0D24N). M.D. and M.T.B. acknowledge funding from a starting grant from the European Research Council (ERC-2020-STG 948449, Z-EURECA). J.D. acknowledges Research Foundation Flanders (FWO Vlaanderen) for funding (Grant 12E4623N). D.S. and R.O.-S. are grateful for the KU Leuven Starting Grant to D.S. and by the Research Foundation Flanders (FWO Vlaanderen) under Grant PorMedNMR (G0D5419N) to D.S. SACHEM is explicitly thanked for providing the organic structure-directing agent (TmAdamOH and TPAOH). The authors thank Prof. Jin Won Seo for her support for TEM imaging/troubleshooting and the Hercules Fund (Project AKUL/13/19) for financial support for the TEM.

■ REFERENCES

(1) Dusselier, M.; Davis, M. E. Small-Pore Zeolites: Synthesis and Catalysis. *Chem. Rev.* **2018**, *118*, 5265−5329.

(2) Cundy, C. S.; Cox, P. A. The Hydrothermal Synthesis of Zeolites: Precursors, Intermediates and Reaction Mechanism. *Microporous Mesoporous Mater.* **2005**, *82*, 1−78.

(3) Barrer, R. M.; Robinson, D. J. KFI Synthesis. *Z. Kristallogr.* **1972**, *135*, 374−390.

(4) Deneyer, A.; Ke, Q.; Devos, J.; Dusselier, M. Zeolite Synthesis under Nonconventional Conditions: Reagents, Reactors, and Modi Operandi. *Chem. Mater.* **2020**, *32*, 4884−4919.

(5) Ivanushkin, G.; Dusselier, M. Engineering Lewis Acidity in Zeolite Catalysts by Electrochemical Release of Heteroatoms during Synthesis. *Chem. Mater.* **2023**, *35*, 5049−5058.

(6) Park, M. B.; Jo, D.; Jeon, H. C.; Nicholas, C. P.; Lewis, G. J.; Hong, S. B. Zeolite Synthesis from a Charge Density Perspective: The Charge Density Mismatch Synthesis of UZM-5 and UZM-9. *Chem. Mater.* **2014**, *26*, 6684−6694.

(7) Lewis, G. J.; Miller, M. A.; Moscoso, J. G.; Wilson, B. A.; Knight, L. M.; Wilson, S. T. Experimental Charge Density Matching Approach to Zeolite Synthesis. In *Studies in Surface Science and Catalysis*; Elsevier, 2004; Vol. *154*, pp 364−372.

(8) Devos, J.; Robijns, S.; Van Goethem, C.; Khalil, I.; Dusselier, M. Interzeolite Conversion and the Role of Aluminum: Toward Generic Principles of Acid Site Genesis and Distributions in ZSM-5 and SSZ-13. *Chem. Mater.* **2021**, *33*, 2516−2531.

(9) Zones, S. I.; Lew, C. M.; Xie, D.; Davis, T. M.; Schmidt, J. E.; Saxton, R. J. Studies on the Use of Faujasite as a Reagent to Deliver Silica and Alumina in Building New Zeolite Structures with Organo-Cations. *Microporous Mesoporous Mater.* **2020**, *300*, No. 110162.

(10) Bickel, E. E.; Nimlos, C. T.; Gounder, R. Developing Quantitative Synthesis-Structure-Function Relations for Framework Aluminum Arrangement Effects in Zeolite Acid Catalysis. *J. Catal.* **2021**, *399*, 75−85.

(11) Bae, J.; Dusselier, M. Synthesis Strategies to Control the Al Distribution in Zeolites: Thermodynamic and Kinetic Aspects. *Chem. Commun.* **2023**, *59*, 852−867.

(12) Lv, W.; Wang, S.; Wang, P.; Liu, Y.; Huang, Z.; Li, J.; Dong, M.; Wang, J.; Fan, W. Regulation of Al Distributions and Cu2+ Locations in SSZ-13 Zeolites for NH3-SCR of NO by Different Alkali Metal Cations. *J. Catal.* **2021**, *393*, 190−201.

(13) Di Iorio, J. R.; Gounder, R. Controlling the Isolation and Pairing of Aluminum in Chabazite Zeolites Using Mixtures of Organic and Inorganic Structure-Directing Agents. *Chem. Mater.* **2016**, *28*, 2236−2247.

(14) Di Iorio, J. R.; Li, S.; Jones, C. B.; Nimlos, C. T.; Wang, Y.; Kunkes, E.; Vattipalli, V.; Prasad, S.; Moini, A.; Schneider, W. F.; Gounder, R. Cooperative and Competitive Occlusion of Organic and Inorganic Structure-Directing Agents within Chabazite Zeolites Influences Their Aluminum Arrangement. *J. Am. Chem. Soc.* **2020**, *142*, 4807−4819.
(15) Robijns, S.; Devos, J.; Donckels, T.; de Oliveira-Silva, R.; De Witte, N.; Sakellariou, D.; Van Assche, T. R. C.; Dusselier, M. Steering Interzeolite Conversion with Alkali Metal Cations: Lithium Maximizes Al Proximity in SSZ-13 Zeolite Genesis. *Cryst. Growth Des.* **2023**, *23*, 289−299.
(16) Devos, J.; Shah, M. A.; Dusselier, M. On the Key Role of Aluminium and Other Heteroatoms during Interzeolite Conversion Synthesis. *RSC Adv.* **2021**, *11*, 26188−26210.
(17) Devos, J.; Bols, M. L.; Plessers, D.; Van Goethem, C.; Seo, J. W.; Hwang, S.-J.; Sels, B. F.; Dusselier, M. Synthesis−Structure−Activity Relations in Fe-CHA for C−H Activation: Control of Al Distribution by Interzeolite Conversion. *Chem. Mater.* **2020**, *32*, 273−285.
(18) Muraoka, K.; Chaikittisilp, W.; Okubo, T. Energy Analysis of Aluminosilicate Zeolites with Comprehensive Ranges of Framework Topologies, Chemical Compositions, and Aluminum Distributions. *J. Am. Chem. Soc.* **2016**, *138*, 6184−6193.
(19) Kosinov, N.; Auffret, C.; Borghuis, G. J.; Sripathi, V. G. P.; Hensen, E. J. M. In Fl Uence of the Si/Al Ratio on the Separation Properties of SSZ-13 Zeolite Membranes. *J. Membr. Sci.* **2015**, *484*, 140−145.
(20) Al Jabri, H.; Miyake, K.; Ono, K.; Nakai, M.; Hirota, Y.; Uchida, Y.; Miyamoto, M.; Nishiyama, N. Synthesis of High Silica SSZ-13 in Fluoride-Free Media by Dry Gel Conversion Method. *Microporous Mesoporous Mater.* **2019**, *278*, 322−326.
(21) Díaz-Cabañas, M.-J.; Barrett, P. A. Synthesis and Structure of Pure SiO2 Chabazite: The SiO2 Polymorph with the Lowest Framework Density. *Chem. Commun.* **1998**, *17*, 1881−1882.
(22) Yang, Y.; Meng, X.; Zhu, L.; Yang, J.; Zhang, G.; Shen, H.; Cao, X. Rapid Synthesis of Si-Rich SSZ-13 Zeolite under Fluoride-Free Conditions. *Inorg. Chem.* **2022**, *61*, 21115−21122.
(23) Ma, C.; Liu, X.; Hong, Y.; Yan, N.; Nie, C.; Wang, J.; Guo, P.; Liu, Z. Fluoride- and Seed-Free Synthesis of Pure-Silica Zeolite Adsorbent and Matrix Using OSDA-Mismatch Approach. *J. Am. Chem. Soc.* **2023**, *145*, 24191−24201.
(24) Aiello, R.; Crea, F.; Nastro, A.; Subotic, B.; Testa, F. Influence of Cations on the Physicochemical and Structural Properties of Aluminosilicate Gel Precursors. I. Chemical and Thermal Properties. *Zeolites* **1991**, *11*, 767−775.
(25) De Witte, N.; Robijns, S.; Denayer, J. F. M.; Dusselier, M.; Van Assche, T. R. C. Inverse Gas Chromatography Study of n - Alkane and 1 - Alkene Adsorption on Pure-Silica LTA (ITQ-29) and CHA. *J. Phys. Chem. C* **2023**, *127*, 24393−24402.
(26) Ertl, G.; Knözinger, H.; Weitkamp, J. *Preparation of Solid Catalysts*, 1st ed.; Wiley-vch: Weinheim, 1999.
(27) Kumar, M.; Choudhary, M. K.; Rimer, J. D. Transient Modes of Zeolite Surface Growth from 3D Gel-like Islands to 2D Single Layers. *Nat. Commun.* **2018**, *9*, No. 2129.
(28) Liu, Z.; Wakihara, T.; Nishioka, D.; Oshima, K.; Takewaki, T.; Okubo, T. One-Minute Synthesis of Crystalline Microporous Aluminophosphate (AlPO4−5) by Combining Fast Heating with a Seed-Assisted Method. *Chem. Commun.* **2014**, *50*, 2526−2528.
(29) Walton, R. I.; Millange, F.; O'Hare, D.; Davies, A. T.; Sankar, G.; Catlow, C. R. A. In Situ Energy-Dispersive X-Ray Diffraction Study of the Hydrothermal Crystallization of Zeolite A. 1. Influence of Reaction Conditions and Transformation into Sodalite. *J. Phys. Chem. B* **2001**, *105*, 83−90.
(30) Kadja, G. T. M.; Azhari, N. J.; Mukti, R. R.; Khalil, M. A Mechanistic Investigation of Sustainable Solvent-Free, Seed-Directed Synthesis of ZSM-5 Zeolites in the Absence of an Organic Structure-Directing Agent. *ACS Omega* **2021**, *6*, 925−933.
(31) Jacobs, P. A. Some Thermodynamic and Kinetic Effects Related to Zeolite Crystallization. In *Zeolite Microporous Solids: Synthesis, Structure, and Reactivity*; Derouane, E. G.; Lemos, F.; Naccache, C.; Ribeiro, F. R., Eds.; springer-science: Dordrecht, 1992; p 643.
(32) Mallette, A. J.; Shilpa, K.; Rimer, J. D. The Current Understanding of Mechanistic Pathways in Zeolite Crystallization. *Chem. Rev.* **2024**, *124*, 3416−3493.
(33) Jain, R.; Mallette, A. J.; Rimer, J. D. Controlling Nucleation Pathways in Zeolite Crystallization: Seeding Conceptual Methodologies for Advanced Materials Design. *J. Am. Chem. Soc.* **2021**, *143*, 21446−21460.
(34) Chen, C. T.; Iyoki, K.; Yamada, H.; Sukenaga, S.; Ando, M.; Shibata, H.; Ohara, K.; Wakihara, T.; Okubo, T. Zeolite Crystallization Triggered by Intermediate Stirring. *J. Phys. Chem. C* **2019**, *123*, 20304−20313.
(35) Jain, R.; Rimer, J. D. Microporous and Mesoporous Materials Seed-Assisted Zeolite Synthesis : The Impact of Seeding Conditions and Interzeolite Transformations on Crystal Structure and Morphology. *Microporous Mesoporous Mater.* **2020**, *300*, No. 110174.
(36) Kumar, M.; Luo, H.; Román-Leshkov, Y.; Rimer, J. D. SSZ-13 Crystallization by Particle Attachment and Deterministic Pathways to Crystal Size Control. *J. Am. Chem. Soc.* **2015**, *137*, 13007−13017.
(37) Qin, W.; Zhou, Y.; Rimer, J. D. Deleterious Effects of Non-Framework Al Species on the Catalytic Performance of ZSM-5 Crystals Synthesized at Low Temperature. *React. Chem. Eng.* **2019**, *4*, 1957−1968.
(38) Asselman, K.; Pellens, N.; Thijs, B.; Doppelhammer, N.; Haouas, M.; Taulelle, F.; Martens, J. A.; Breynaert, E.; Kirschhock, C. E. A. Ion-Pairs in Aluminosilicate-Alkali Synthesis Liquids Determine the Aluminum Content and Topology of Crystallizing Zeolites. *Chem. Mater.* **2022**, *34*, 7150−7158.
(39) Bordiga, S.; Lamberti, C.; Bonino, F.; Travert, A.; Thibault-Starzyk, F. Probing Zeolites by Vibrational Spectroscopies. *Chem. Soc. Rev.* **2015**, *44*, 7262−7341.
(40) Medeiros-Costa, I. C.; Dib, E.; Nesterenko, N.; Dath, J. P.; Gilson, J. P.; Mintova, S. Silanol Defect Engineering and Healing in Zeolites: Opportunities to Fine-Tune Their Properties and Performances. *Chem. Soc. Rev.* **2021**, *50*, 11156−11179.
(41) Engelhardt, G.Solid State NMR Spectroscopy Applied to Zeolites. In *Studies in Surface Science and Catalysis*; Elsevier, 2001; Vol. *137*, pp 387−418.
(42) Shin, J.; Ahn, N. H.; Camblor, M. A.; Cho, S. J.; Hong, S. B. Intraframework Migration of Tetrahedral Atoms in a Zeolite. *Angew. Chem., Int. Ed.* **2014**, *53*, 8949−8952.
(43) Lee, S.; Nimlos, C. T.; Kipp, E. R.; Wang, Y.; Gao, X.; Schneider, W. F.; Lusardi, M.; Vattipalli, V.; Prasad, S.; Moini, A.; Gounder, R. Evolution of Framework Al Arrangements in CHA Zeolites during Crystallization in the Presence of Organic and Inorganic Structure-Directing Agents. *Cryst. Growth Des.* **2022**, *22*, 6275−6295.
(44) Dědeček, J.; Kaukcy, D.; Wichterlová, B.; Gonsiorova, O. Co2+ Ions as Probes of Al Distribution in the Framework of Zeolites. ZSM-5 Study. *Phys. Chem. Chem. Phys.* **2002**, *4*, 5406−5413.
(45) Di Iorio, J. R.; Nimlos, C. T.; Gounder, R. Introducing Catalytic Diversity into Single-Site Chabazite Zeolites of Fixed Composition via Synthetic Control of Active Site Proximity. *ACS Catal.* **2017**, *7*, 6663−6674.
(46) Bellmann, A.; Rautenberg, C.; Bentrup, U.; Brückner, A. Determining the Location of Co2+ in Zeolites by UV-Vis Diffuse Reflection Spectroscopy: A Critical View. *Catalysts* **2020**, *10*, No. 123.
(47) Devos, J.; Bols, M. L.; Plessers, D.; Van Goethem, C.; Seo, J. W.; Hwang, S. J.; Sels, B. F.; Dusselier, M. Synthesis-Structure-Activity Relations in Fe-CHA for C-H Activation: Control of Al Distribution by Interzeolite Conversion. *Chem. Mater.* **2020**, *32*, 273−285.
(48) Flores-Granobles, M.; Saeys, M. Quantitative Analysis of CO2 Emissions Reduction Potential of Alternative Light Olefins Production Processes. *Green Chem.* **2023**, *25*, 6459−6471.
(49) Shi, Z.; Neurock, M.; Bhan, A. Methanol-to-Olefins Catalysis on HSSZ-13 and HSAPO-34 and Its Relationship to Acid Strength. *ACS Catal.* **2021**, *11*, 1222−1232.
(50) Zhao, X.; Li, J.; Tian, P.; Wang, L.; Li, X.; Lin, S.; Guo, X.; Liu, Z. Achieving a Superlong Lifetime in the Zeolite-Catalyzed MTO

Reaction under High Pressure: Synergistic Effect of Hydrogen and Water. *ACS Catal.* **2019**, *9*, 3017−3025.
(51) Devos, J.; Borms, R.; Robijns, S.; Ivanushkin, G.; Khalil, I.; Dusselier, M. Engineering Low-Temperature Ozone Activation of Zeolites: Process Specifics, Possible Mechanisms and Hybrid Activation Methods. *Chem. Eng. J.* **2022**, *431*, No. 133862.
(52) Chernyak, S. A.; Corda, M.; Marinova, M.; Safonova, O. V.; Kondratenko, V. A.; Kondratenko, E. V.; Kolyagin, Y. G.; Cheng, K.; Ordomsky, V. V.; Khodakov, A. Y. Decisive Influence of SAPO-34 Zeolite on Light Olefin Selectivity in Methanol-Meditated CO2 Hydrogenation over Metal Oxide-Zeolite Catalysts. *ACS Catal.* **2023**, *13*, 14627−14638.
(53) Di, W.; Achour, A.; Ho, P. H.; Ghosh, S.; Pajalic, O.; Josefsson, L.; Olsson, L.; Creaser, D. Modulating the Formation of Coke to Improve the Production of Light Olefins from CO2 Hydrogenation over In2O3 and SSZ-13 Catalysts. *Energy Fuels* **2023**, *37*, 17382−17398.
(54) Chen, S.; Wang, J.; Feng, Z.; Jiang, Y.; Hu, H.; Qu, Y.; Tang, S.; Li, Z.; Liu, J.; Wang, J.; Li, C. Hydrogenation of CO 2 to Light Olefins over ZnZrO x /SSZ-13. *Angew. Chem., Int. Ed.* **2024**, *63*, No. e202316874.
(55) Mallette, A. J.; Espindola, G.; Varghese, N.; Rimer, J. D. Highly Efficient Synthesis of Zeolite Chabazite Using Cooperative Hydration-Mismatched Inorganic Structure-Directing Agents. *Chem. Sci.* **2024**, *15*, 573−583.
(56) Arroyo, R. D.; Pascual, J.; Jensen, K.; Hwang, S.-J.; Zones, S. I. Studies on the Conversion of FAU Zeolites to SSZ-13: The Rate Advantage of Having Both Si and Al in the FAU Reagent. *Cryst. Growth Des.* **2023**, *23*, 6318−6330.
(57) Nakagawa, Y.; Lee, G. S.; Harris, T. V.; Yuen, L. T.; Zones, S. I. Guest/Host Relationships in Zeolite Synthesis: Ring-Substituted Piperidines and the Remarkable Adamantane Mimicry by 1-Azonio Spiro [5.5] Undecanes. *Microporous Mesoporous Mater.* **1998**, *22*, 69−85.
(58) Ennaert, T.; Van Aelst, J.; Dijkmans, J.; De Clercq, R.; Schutyser, W.; Dusselier, M.; Verboekend, D.; Sels, B. F. Potential and Challenges of Zeolite Chemistry in the Catalytic Conversion of Biomass. *Chem. Soc. Rev.* **2016**, *45*, 584−611.
(59) De Yoreo, J. J. Principles of Crystal Nucleation and Growth. *Rev. Mineral. Geochem.* **2003**, *54*, 57−93.
(60) Chen, C. T.; Iyoki, K.; Hu, P.; Yamada, H.; Ohara, K.; Sukenaga, S.; Ando, M.; Shibata, H.; Okubo, T.; Wakihara, T. Reaction Kinetics Regulated Formation of Short-Range Order in an Amorphous Matrix during Zeolite Crystallization. *J. Am. Chem. Soc.* **2021**, *143*, 10986−10997.

https://doi.org/10.1021/jacsau.4c00551
JACS Au 2025, 5, 593−605